Metadata of the chapter that will be visualized in SpringerLink

Book Title	Advanced Nondestructive and Structural Techniques for Diagnosis, Redesign and Health Monitoring for the Preservation of Cultural Heritage
Series Title	
Chapter Title	Artificial Intelligence Analysis of Macroscopic X-Ray Fluorescence Data: A Case Study of Nineteenth Century Icon
Copyright Year	2024
Copyright HolderName	The Author(s), under exclusive license to Springer Nature Switzerland AG

Corresponding Author	Family Name	**Gerodimos**
	Particle	
	Given Name	**T.**
	Prefix	
	Suffix	
	Role	
	Division	Department of Material Science and Engineering
	Organization	University of Ioannina
	Address	Ioannina, Greece
	Email	fgerodim@uoi.gr
Author	Family Name	**Chatzipanteliadis**
	Particle	
	Given Name	**D.**
	Prefix	
	Suffix	
	Role	
	Division	Department of Material Science and Engineering
	Organization	University of Ioannina
	Address	Ioannina, Greece
	Email	
Author	Family Name	**Chantas**
	Particle	
	Given Name	**G.**
	Prefix	
	Suffix	
	Role	
	Division	Department of Computer Science and Engineering
	Organization	University of Ioannina
	Address	Ioannina, Greece
	Email	
Author	Family Name	**Asvestas**
	Particle	
	Given Name	**A.**
	Prefix	

	Suffix	
	Role	
	Division	Department of Material Science and Engineering
	Organization	University of Ioannina
	Address	Ioannina, Greece
	Email	
Author	Family Name	**Mastrotheodoros**
	Particle	
	Given Name	**G.**
	Prefix	
	Suffix	
	Role	
	Division	Department of Material Science and Engineering
	Organization	University of Ioannina
	Address	Ioannina, Greece
	Division	Department of Conservation of Antiquities and Works of Art
	Organization	West Attica University
	Address	Aigaleo, Greece
	Email	
Author	Family Name	**Likas**
	Particle	
	Given Name	**A.**
	Prefix	
	Suffix	
	Role	
	Division	Department of Computer Science and Engineering
	Organization	University of Ioannina
	Address	Ioannina, Greece
	Email	
Author	Family Name	**Anagnostopoulos**
	Particle	
	Given Name	**D. F.**
	Prefix	
	Suffix	
	Role	
	Division	Department of Material Science and Engineering
	Organization	University of Ioannina
	Address	Ioannina, Greece
	Email	

Abstract

This work comprehensively reviews artificial intelligence (AI) methods for macroscopic X-ray fluorescence (MA-XRF) data analysis of a religious panel painting (icon). MA-XRF is a powerful analytical imaging technique used to determine the elemental distribution maps of inhomogeneous targets. For the data analysis, we apply clustering algorithms such as k-means, factorization methods such as principal component analysis (PCA) and non-negative matrix factorization (NMF), and basic supervised machine learning methods, such as k-nearest neighbor (k-NN) regression and multilayer perceptron (MLP) regression. The applied AI methods allow for detailed and fast data analysis, providing two-dimensional elemental maps. The methods are beneficial for inexperienced users as they can analyze the MA-XRF data without detailed knowledge of the involved physics.

Keywords (separated by '-')	MA-XRF - Spectral analysis - Elemental maps - Clustering algorithms - Matrix factorization - Artificial neural networks - Cultural heritage

Artificial Intelligence Analysis of Macroscopic X-Ray Fluorescence Data: A Case Study of Nineteenth Century Icon

T. Gerodimos, D. Chatzipanteliadis, G. Chantas, A. Asvestas, G. Mastrotheodoros, A. Likas, and D. F. Anagnostopoulos

Abstract This work comprehensively reviews artificial intelligence (AI) methods for macroscopic X-ray fluorescence (MA-XRF) data analysis of a religious panel painting (icon). MA-XRF is a powerful analytical imaging technique used to determine the elemental distribution maps of inhomogeneous targets. For the data analysis, we apply clustering algorithms such as k-means, factorization methods such as principal component analysis (PCA) and non-negative matrix factorization (NMF), and basic supervised machine learning methods, such as k-nearest neighbor (k-NN) regression and multilayer perceptron (MLP) regression. The applied AI methods allow for detailed and fast data analysis, providing two-dimensional elemental maps. The methods are beneficial for inexperienced users as they can analyze the MA-XRF data without detailed knowledge of the involved physics.

Keywords MA-XRF · Spectral analysis · Elemental maps · Clustering algorithms · Matrix factorization · Artificial neural networks · Cultural heritage

T. Gerodimos (✉) · D. Chatzipanteliadis · A. Asvestas · G. Mastrotheodoros · D. F. Anagnostopoulos
Department of Material Science and Engineering, University of Ioannina, Ioannina, Greece
e-mail: fgerodim@uoi.gr

G. Chantas · A. Likas
Department of Computer Science and Engineering, University of Ioannina, Ioannina, Greece

G. Mastrotheodoros
Department of Conservation of Antiquities and Works of Art, West Attica University, Aigaleo, Greece

A. Osman et al. (eds.), *Advanced Nondestructive and Structural Techniques for Diagnosis, Redesign and Health Monitoring for the Preservation of Cultural Heritage*, Springer Proceedings in Materials 33,
https://doi.org/10.1007/978-3-031-42239-3_3

1 Introduction

X-ray fluorescence spectroscopy (XRF) has wide application in investigating cultural heritage items because it allows for a rapid, accurate, and non-invasive elemental characterization [1]. X-rays penetrate deeper into matter than visible light. Recent advances led to the development of macroscopic XRF scanners (MA-XRF) that collect and process up to millions of successive spectra, scanning on the fly a predefined surface [2–4]. MA-XRF measurements produce big data that needs careful analysis to extract precise and accurate results. The outcome of the analysis is two-dimensional elemental maps across the scanned area. Applying MA-XRF for the study of paintings allows the extraction of elemental maps, which provide information about the pigments used and paint layer stratigraphy (i.e., painting technique) as well as restoration interventions/state of preservation [5, 6]. State-of-the-art analysis techniques are mandatory to analyze the vast amount of data produced. The advancements in computer science, specifically in artificial intelligence, will significantly boost the analysis of MA-XRF data. Application of AI methods, like clustering, factorization, and advanced machine learning algorithms, such as artificial neural networks, is expected to tackle essential issues, like time of analysis and unattended results interpretation by non-experienced users [7–11]. The current work demonstrates the potentialities of fundamental AI algorithms by investigating a Greek Orthodox Christian religious panel painting (“icon”).

2 Materials and Methods

2.1 Instrumentation and Measurement

The potentialities of all proposed methods are explored through the examination of a 19th-century Greek “two-zone icon” that depicts a “Deesis” scene (upper zone) and various Saints (lower zone) with dimensions of 46 × 32 cm^2.

The MA-XRF measurement was realized with the M6-Jetstream (Bruker) scanner [12, 13], which allows scan areas 80 × 60 cm^2. The M6 Jetstream is equipped with a 30 W Rhodium X-ray tube. In the present measurement, the X-ray tube was operated at a high voltage of 50 kV and a current of 600 μA, while no absorption filter was applied on the beam path of the ionization radiation. The incoming from the source X-ray beam is focused using a polycapillary glass optic and impinges perpendicularly to the target surface. The excitation beam spot size had a diameter of 580 μm. The sensor detects photons emerging at an angle of 60° relative to the target surface. A silicon drift detector of 30 mm^2 active area is used for the photon detection, with an energy resolution of 145 eV at the Mn Kα-energy. A total of 202 × 318 mm^2 were scanned (upper zone—“Deesis”), as shown in Fig. 1 (left), with a pixel size of 1000 μm. The dwell time was 10 ms per pixel and the overall measurement time was ~15 min. Each spectrum consists of 4096 channels, while a total of 64,236 spectra

546446_1_En_3_Chapter ☑ TYPESET ☐ DISK ☐ LE ☑ CP Disp.:25/8/2023 Pages: ?? Layout: T1-Standard

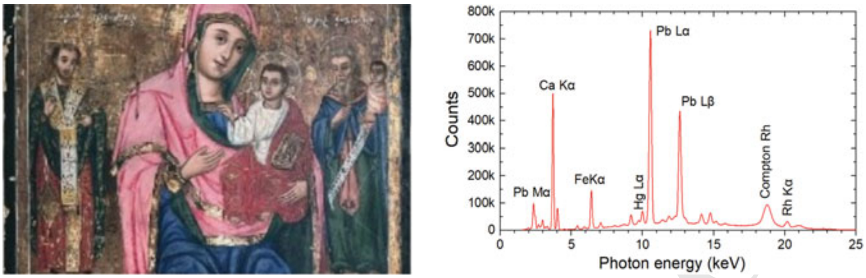

Fig. 1 Left: Scanned image; Right: Sum spectrum of the scanned image

were collected and the corresponding sum spectrum is shown in Fig. 1 (right). The dominant observed elements are Pb, Fe, Ca and Hg.

2.2 Artificial Intelligence Applied Methods

On one hand, PCA and NMF are machine-learning techniques that can be applied to XRF spectra to extract useful information and patterns from the data. PCA is a dimensionality reduction technique that reduces the number of variables in a dataset while preserving as much of the variation in the data as possible [14]. In the context of XRF spectra, PCA can identify the highest intensities X-ray transitions that contribute to the spectra structure [15]. NMF is a widely used technique for factorizing a matrix into the product of two non-negative matrices [16]. In the context of XRF spectra, NMF can decompose the spectra into a set of “basis spectra”, each corresponding to a different elemental component. Both PCA and NMF can be useful for identifying a material’s dominant elemental components or detecting subtle differences in elemental composition between samples [17, 18].

Clustering, on the other hand, is a technique that groups similar data points together into clusters. With clustering algorithms in XRF spectra, we can identify unknown materials or detect outliers in a dataset. The main objective of clustering methods in XRF analysis is the grouping of similar in-shape spectra in distinct clusters corresponding to areas with comparable elemental composition. The cluster formation is based on the relative intensities of the spectral lines [19, 20].

Artificial Intelligence Networks (ANNs) are a group of machine learning algorithms that can learn how to predict elemental distribution intensity from a set of training data, such as XRF spectra in our case. Weighted k-nearest neighbors (k-NN) and multilayer perceptron (MLP) are two different types of machine learning algorithms that can be used for MA-XRF elemental distribution map prediction.

Weighted k-NN is an extension of the k-NN algorithm, in which the prediction is computed as the weighted average of the values of the k nearest neighbors. The weight of each neighbor is calculated as the inverse of its distance to the test point so that closer neighbors have a more significant influence on the prediction than more distant neighbors. This allows the model to give more importance to the points closest to the test point, which can be helpful when the data has a non-uniform distribution or when there is noise in the dataset.

MLP is a feed-forward artificial neural network composed of an input layer, one or more hidden layers, and an output layer. Each layer is made up of a set of artificial neurons, which are connected to the neurons in the adjacent layers via a set of weights. The network learns to make predictions by adjusting the weights to minimize the error between the predicted output and the ground truth during training [21, 22]. In this context, ANN's can be used to predict the elemental distribution maps from XRF data by performing regression of the output elemental distribution maps.

3 Results and Discussion

3.1 Matrix Factorization Analysis

For the matrix factorization analysis, we consider the measured XRF spectra as a three-dimensional "data cube". A data cube $X(4096 \times 202 \times 318)$ consists of two spatial dimensions (representing the x and y axis' pixels of the image in consideration) and one energy dimension representing the spectrum associated with each pixel. With the use of NMF, we decomposed the data cube into the product of two non-negative matrices, ($X = W \times H$), where W is a 2-dimensional matrix (4096×6) representing the "basis spectra", and H is a 3-dimensional matrix ($6 \times 202 \times 318$) representing the "basis images". The "basis images" give information about the spatial distribution of the elements, while the "basis spectra" provide information about the XRF spectrum of each component. PCA method was also used with the same approach [15]. Python's sklearn module was used for both methods [23], and the results are shown in Figs. 2 and 3.

The data were analyzed using PyMca (version 5.6.7) [24] and the main elements were identified. Thus, for each pixel-spectra, a ground truth elemental composition with the intensities per element was created, thus providing the distribution map for

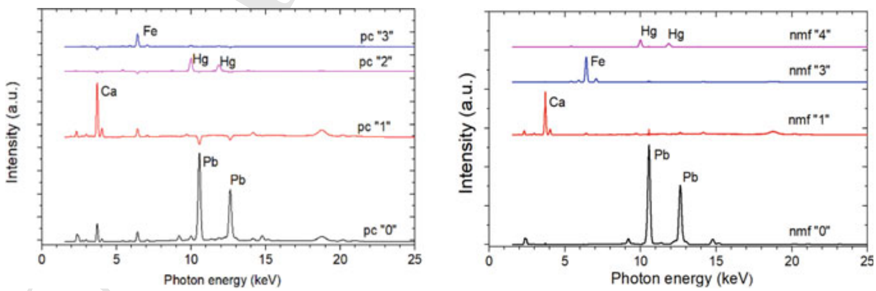

Fig. 2 Set of "basis spectra" according to the PCA (left) and the NMF analysis (right)

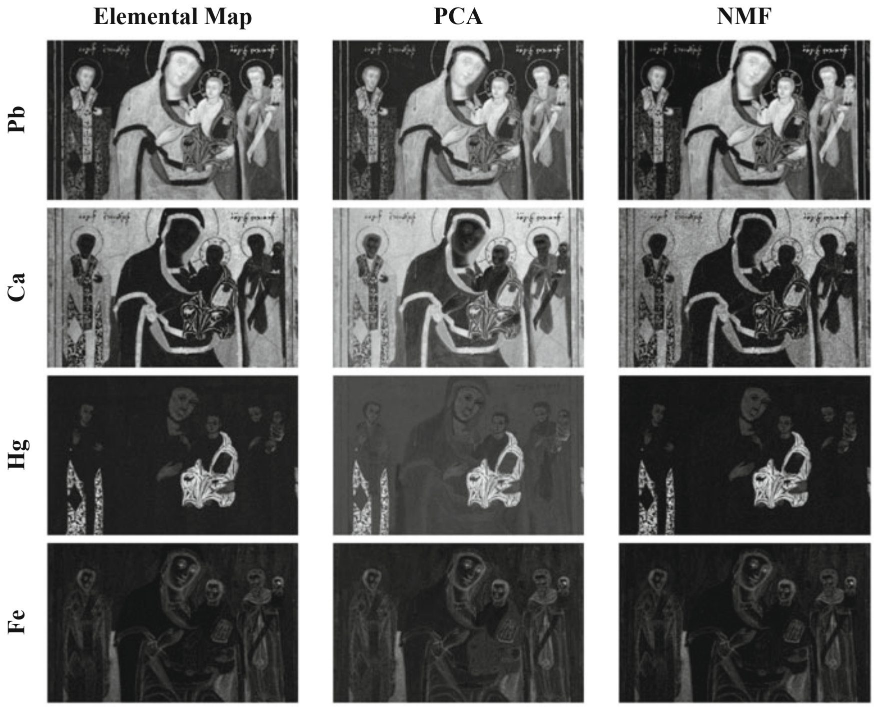

Fig. 3 Elemental maps according to PyMca analysis (ground trurh/left), and subset of "basis images" according to PCA (center) and NMF (right) analysis

each of the elements presented in the painting. For instance, Fig. 3 (left) shows the elemental maps of Pb, Ca, Hg and Fe as they emerged from the analysis.

Both methods effectively produced elemental distribution maps and identified patterns and structures in the data. As shown in Fig. 2 methods yield spectra with peaks that are perfectly aligned with the XRF excitation energies sum spectrum. Also, as we show in the maps of Fig. 3, the main elements of the icons are in good agreement with the ground truth results. Especially the Pb and Fe elemental maps extracted by the factorization methods are in excellent agreement with the ground truth analysis, while there some concerning the Ca's map. One of the most interesting findings in this study is the comparison of the performance of PCA and NMF in identifying Hg, an element with low concentration in the panel painting, as shown in the sum spectrum (Fig. 1). Despite the low concentration, NMF could accurately identify Hg, while PCA performed poorly. This suggests that NMF may be more robust to low concentration levels and that it should be considered a viable alternative when analyzing elemental distribution maps containing trace elements.

3.2 Cluster Analysis

The well-known k-means clustering algorithm [25, 26] was selected for the dataset analysis due to its simplicity and low computational complexity. The measured spectra were grouped into six non-overlapping groups. As inferred from the sum spectrum (Fig. 1) and the ground truth elemental maps (Fig. 3, left), Pb and Ca are dominating the painting. For this reason, and as intensities have nonnegative values, we apply the square root function to the intensity of the data set during the cluster analysis. Square root transformation can help reduce the effect of high-intensity pixels, which can disproportionately affect the clustering results dominating the cluster centers.

For each cluster, the mean spectrum was evaluated (Fig. 4, left), providing significantly better statistics than any single-pixel spectrum of the data set. The mean spectrum represents areas of similar composition, thus allowing the accurate identification of the elements' presence. This, in turn, permits the extraction of information about the used pigments, paint layer stratigraphy, painting technique, previous restoration interventions, and state of preservation of each area of the panel painting in consideration [10, 11].

Two clusters ("1" and "2") are dominated by the Ca Kα intensities, while in cluster "1" the transition lines of Pb appear as well. In both clusters Fe (at 6.4 keV) is also present. In traditional icon painting, craftsmen always covered the wooden substrates with successive gesso layers; the latter was made by mixing gypsum ($CaSO_4 \cdot 2H_2O$) with animal glue [27]. The Ca transition lines are weak to the rest of the clusters due to their absorption by the superimposed paint layers in the areas where the gesso has been covered by heavy element-based pigments, such as lead white and cinnabar. Nevertheless, minor calcium is often detected in various (primarily earth) pigments.

Four clusters ("0", "3", "4", and "5") are dominated by the Pb Lα and Lβ intensities. In cluster "4," there are intense Hg L transitions and the weak K transition of Cr and Fe at 5.4 keV and 6.4 keV, respectively. The cluster corresponds to the bright-red colored areas, and the identified elements suggest using a red lead chromate plus cinnabar pigment mixture to render these areas [28]. Cluster "0" corresponds

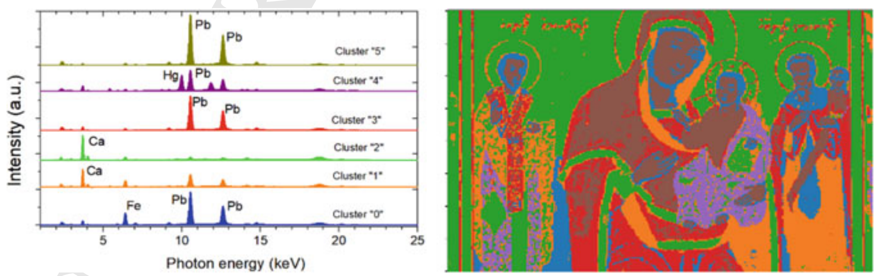

Fig. 4 Left: Cluster mean spectra, Right: Spatial distribution per cluster

to flesh areas. There is an intense Fe K transition, indicating the admixture of ochre to provide the dark tone in lead white [11].

3.3 k-NN Regression

For the k-NN regression algorithm, we first select a representative part, i.e., containing all the elements of the icon under study (columns 170–190 as denoted by the blue stripe in Fig. 5), corresponding to 6.3% of the total pixels. It is important to note at this point that each pixel-spectrum X_i corresponds to a vector-target y_i with the intensities of the elements derived from the XRF analysis.

Following this, we employ the k-NN regression algorithm with weights, with a value of k equal to 5, on the whole image and check the results given to verify the presence of the elements in the remaining regions of the painting. To evaluate the performance of the proposed method, we utilize the Structural Similarity Index (SSIM) [29] as a widely accepted metric for assessing the quality of the results obtained. The SSIM is a widely used quality index for image comparison that compares the structural information and pixel-level variations between the elemental distribution maps produced by the k-NN algorithm and the ground truth. It provides a value between -1 and 1, where 1 indicates a perfect match and values closer to -1 indicate significant dissimilarity. Figure 5 shows the results of the k-NN algorithm for the four dominant chemical elements (Pb, Ca, Hg, Fe). SSIM index scored pretty good results ranging between 0 and 1, with most of its values towards the higher end of the scale. This is particularly evident at the left edge of the images, where the SSIM value is closed to 0. This observation can be logically explained by the fact that the region in question pertains to a border area between distinct elements, potentially even the edge of the image itself.

3.4 MLP Regression

The MLP regressor consists of an input layer of 4096 neurons, like the spectra size, one hidden layer of 100 neurons, respectively, and finally, an output layer of 12 neurons, one per chemical element. The activation function used for the hidden layer was ReLU, and Adam was set as an optimizer with a learning rate of 0.001. As a loss function, L2 was used, and the training lasted 381 epochs as the training loss did not improve more than a tolerance threshold of 0.0001 for ten consecutive epochs.

The results (Fig. 6) showed that the MLP Regressor performed better than the k-NN Regressor in terms of SSIM score (in all four elements scored more than 0.9), indicating that it was able to predict the elemental distribution maps with a higher degree of accuracy and structural similarity to the ground truth maps. It seems possible that the MLP Regressor, being a more complicated neural network, has a larger capacity to learn from the data and model more complex relationships and

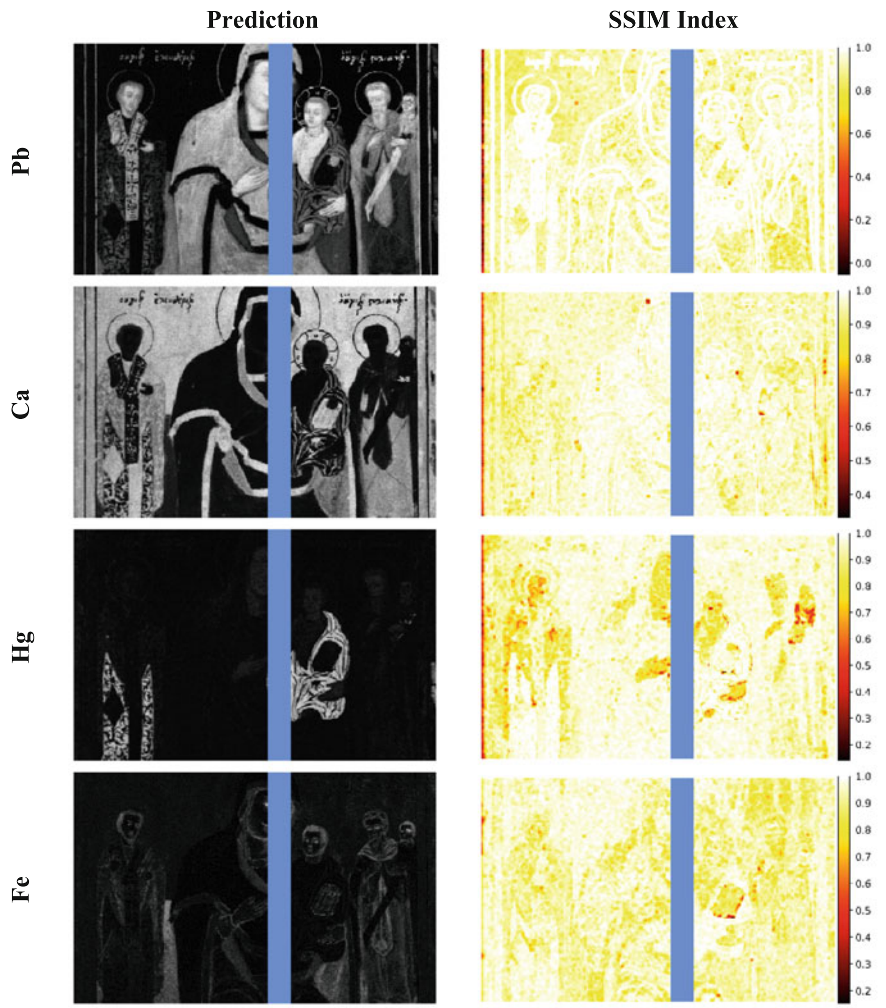

Fig. 5 Left: k-NN regression algorithm predicted elemental maps for Pb, Ca, Hg, and Fe; Right: SSIM index score of k-NN regression algorithm per element. In blue is denoted the area used for the training

correlations between the input spectra and the output elemental distribution maps. Also, MLP demonstrated better ability for generalization handle better variations and possible errors in the data, something especially evident in the left part of the image. In contrast, the k-NN Regressor is a simpler model that may not be able to capture the same level of complexity.

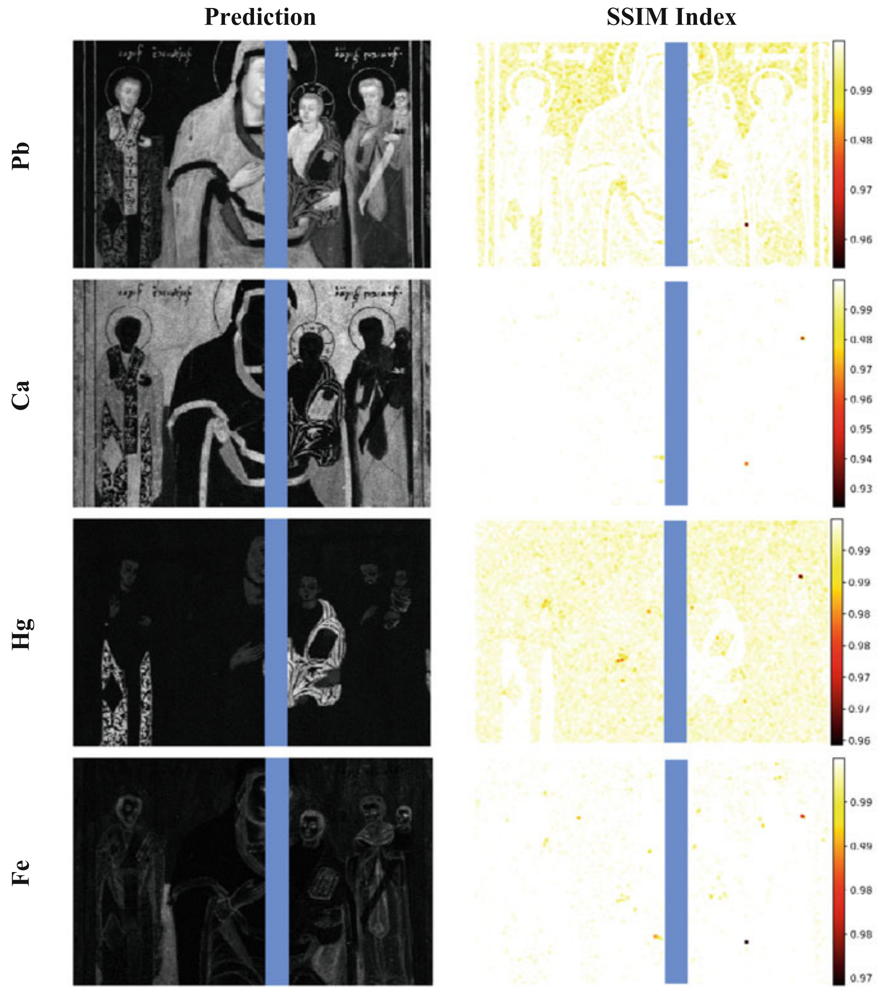

Fig. 6 Left: MLP regression algorithm predicted elemental maps for Pb, Ca, Hg, and Fe; Right: SSIM index score of k-NN regression algorithm per element. In blue is denoted the area used for the training

4 Conclusion

In the present work, we investigated AI techniques to analyze big data created during MA-XRF imaging experiments. Specifically, we applied matrix factorization techniques, like PCA and NMF, to obtain "basis elemental maps" via dimensionality reduction. This approach allowed the computational extraction of elemental distribution maps, which highly agree with the elemental maps extracted by complete XRF spectroscopic analysis. It is worth to be noted that PCA and NMF, being unsupervised methods, provide similar results with the XRF analysis methodology. Moreover, we applied k-means clustering to pack thousands of spectra of similar structures in a small number of representative mean spectra. The clustering identifies areas with similar elemental distribution, composition, and elemental correlation. Moreover, the significantly higher statistics of the cluster's mean spectrum allow not only the detection and identification of the dominant elements, but also trace elements from weak transition lines. Finally, k-NN and MLP regression algorithms were applied to predict the elemental distribution from the MA-XRF spectra. A representative part of a nineteenth century icon was used to train the neural network methods to predict the elemental distribution. The predicted by the NN elemental maps is in remarkable agreement with the ground truth elemental distributions. In conclusion, the present study indicates that the AI methods are up-and-coming for the analysis of MA-XRF big data, as they are significantly faster than the spectroscopic analysis and particularly useful for inexperienced users, as there are no requirements for the involved physics. This makes the investigation for efficient AI algorithms, combined with the variety of MA-XRF big data, highly desirable.

Acknowledgements This research was supported by project "Dioni: Computing Infrastructure for Big-Data Processing and Analysis" (MIS No. 5047222) co-funded by European Union (ERDF) and Greece through Operational Program "Competitiveness, Entrepreneurship and Innovation", NSRF 2014–2020.

Special thanks are due to M. Ziagkos for providing access to icon from private collection.

References

1. Mantler M, Schreiner M (2000) X-ray fluorescence spectrometry in art and archaeology. X-Ray Spectrom: Int J 29(1):3–17
2. Janssens K, Van der Snickt G, Vanmeert F, Legrand S, Nuyts G, Alfeld M, Monico L, Anaf W, De Nolf W, Vermeulen M, Verbeeck J, De Wael K (2016) Non-invasive and non-destructive examination of artistic pigments, paints, and paintings by means of X-ray methods. Top Curr Chem 374(81). https://doi.org/10.1007/s41061-016-0079-2
3. Romano FP, Caliri C, Nicotra P, Di Martino S, Pappalardo L, Rizzo F, Santos HC (2017) Real-time elemental imaging of large dimension paintings with a novel mobile macro X-ray fluorescence (MA-XRF) scanning technique. J Anal At Spectrom 32:773–781
4. Alfeld M, Mösl K, Reiche I (2021) Sunset and moonshine: variable blue and yellow pigments used by Caspar David Friedrich in different creative periods revealed by in situ XRF imaging. X-Ray Spectrom 50(4):341–350
5. Delaney JK, Dooley KA, Van Loon A, Vandivere A (2020) Mapping the pigment distribution of Vermeer's Girl with a Pearl Earring. Herit Sci 8(1):1–16
6. Saverwyns S, Currie C, Lamas-Delgado E (2018) Macro X-ray fluorescence scanning (MA-XRF) as tool in the authentication of paintings. Microchem J 137:139–147
7. Shugar A (2021) Advancements in portable and lab based XRF instrumentation for analysis in cultural heritage: a change in perspective. Microsc Microanal 27(S1):2552–2553
8. Xu BJ, Wu Y, Hao P, Vermeulen M, McGeachy A, Smith K, Walton M et al (2022) Can deep learning assist automatic identification of layered pigments from XRF data?. J Anal At Spectrom 37(12):2672–2682

9. Chopp H, McGeachy A, Alfeld M, Cossairt O, Walton M, Katsaggelos A (2022) Image processing perspectives of X-ray fluorescence data in cultural heritage sciences. IEEE BITS Inf Theory Mag 2(1):20–35
10. Kogou S, Lee L, Shahtahmassebi G, Liang H (2021) A new approach to the interpretation of XRF spectral imaging data using neural networks. X-Ray Spectrom 50(4):310–319
11. Gerodimos T, Asvestas A, Mastrotheodoros GP, Chantas G, Liougos I, Likas A, Anagnostopoulos DF (2022) Scanning X-ray fluorescence data analysis for the identification of byzantine icons' materials, techniques, and state of preservation: a case Study. J Imaging 8(5):147
12. Alfeld M, Pedroso JV, van Eikema Hommes M, Van der Snickt G, Tauber G, Blaas J, Janssens K (2013) A mobile instrument for in situ scanning macro-XRF investigation of historical paintings. J Anal At Spectrom 28(5):760–767
13. https://www.bruker.com/en/products-and-solutions/elemental-analyzers/micro-xrf-spectrometers/m6-jetstream.html
14. Abdi H, Williams LJ (2010) Principal component analysis. Wiley Interdiscip Rev: Comput Statis 2(4):433–459
15. Łach B, Fiutowski T, Koperny S, Krupska-Wolas P, Lankosz M, Mendys-Frodyma A, Dąbrowski W et al (2021) Application of factorisation methods to analysis of elemental distribution maps acquired with a full-field XRF imaging spectrometer. Sensors 21(23):7965
16. Cichocki A, Phan AH (2009) Fast local algorithms for large-scale nonnegative matrix and tensor factorizations. IEICE Trans Fundam Electron Commun Comput Sci 92(3):708–721
17. Alfeld M, Wahabzada M, Bauckhage C, Kersting K, Wellenreuther G, Falkenberg G (Apr 2014) Non-negative factor analysis supporting the interpretation of elemental distribution images acquired by XRF. In: Journal of physics: conference series, vol 499, no 1. IOP Publishing, p 012013
18. Magkanas G, Bagán H, Sistach MC, García JF (2021) Illuminated manuscript analysis methodology using MA-XRF and NMF: application on the Liber Feudorum Maior. Microchem J 165:106112
19. Mihalić IB, Fazinić S, Barac M, Karydas AG, Migliori A, Doračić D, Krstić D et al (2021) Multivariate analysis of PIXE+XRF and PIXE spectral images. J Anal At Spectrom 36(3):654–667
20. Orsilli J, Galli A, Bonizzoni L, Caccia M (2021) More than XRF mapping: STEAM (Statistically Tailored Elemental Angle Mapper) a pioneering analysis protocol for pigment studies. Appl Sci 11:1446
21. Kingma DP, Ba J (2014) Adam: a method for stochastic optimization. arXiv:1412.6980
22. He K, Zhang X, Ren S, Sun J (2015) Delving deep into rectifiers: surpassing human-level performance on imagenet classification. In: Proceedings of the IEEE international conference on computer vision, pp 1026–1034
23. Pedregosa F, Varoquaux G, Gramfort A, Michel V, Thirion B, Grisel O, Duchesnay E et al (2011) Scikit-learn: machine learning in python. J Mach Learn Res 12:2825–2830
24. Solé VA, Papillon E, Cotte M, Walter P, Susini J (2007) A multiplatform code for the analysis of energy-dispersive X-ray fluorescence spectra. Spectrochim Acta Part B: AtIc Spectrosc 62(1):63–68
25. MacQueen J (1967) Classification and analysis of multivariate observations. In: 5th Berkeley symposium on mathematical statistics and probability, pp 281–297
26. Likas A, Vlassis N, Verbeek JJ (2003) The global k-means clustering algorithm. Pattern Recogn 36(2):451–461
27. Mastrotheodoros GP, Beltsios KG, Bassiakos Y, Papadopoulou V (2016) On the grounds of post-byzantine Greek icons. Archaeometry 58(5):830–847
28. Kühn H, Curran M (1986) Chrome yellow and other chromate pigments. In: Feller RL (ed)Artist's pigments: a handbook of their history and characteristics. National Gallery of Art, Cambridge University Press: Cambridge, UK, pp 186–217
29. Wang Z, Bovik AC, Sheikh HR, Simoncelli EP (2004) Image quality assessment: from error visibility to structural similarity. IEEE Trans Image Process 13(4):600–612